Zhang et al. *Zool. Res.* 2026, 47(3): 1003−1014
https://doi.org/10.24272/j.issn.2095-8137.2025.606
https://cstr.cn/32248.14.zr.2025.606

ZR | Zoological Research

Article Open Access

Lethal VSV-based surrogate mouse models for Sudan and Bundibugyo ebolaviruses enable antibody evaluation under BSL-2 conditions

Bao-Yue Zhang[1,2,#], Fang-Xu Li[1,2,#], Shen Wang[3], Jun-Hui Zhou[1,2], Jin-Ge Zhou[1,2], Yan Wu[1], Ying Xie[4], Wu-Jian Li[5,6,7], Fei-Hu Yan[3,*], Xing-Hai Zhang[1,*], Sandra Chiu[5,6,7,*]

[1] *State Key Laboratory of Virology and Biosafety*, *Wuhan Institute of Virology*, *Chinese Academy of Sciences*, *Wuhan*, *Hubei* 430062, *China*

[2] *University of Chinese Academy of Sciences*, *Beijing* 100049, *China*

[3] *Key Laboratory of Jilin Province for Zoonosis Prevention and Control*, *Changchun Veterinary Research Institute*, *Chinese Academy of Agricultural Sciences*, *Changchun*, *Jinlin* 130122, *China*

[4] *Hebei Key Lab of Laboratory Animal Science*, *Department of Laboratory Animal Science*, *Hebei Medical University*, *Shijiazhuang*, *Hebei* 050017, *China*

[5] *Department of Infectious Disease*, *the First Affiliated Hospital of USTC*, *Division of Life Sciences and Medicine*, *University of Science and Technology of China*, *Hefei*, *Anhui* 230027, *China*

[6] *Division of Life Sciences and Medicine*, *University of Science and Technology of China*, *Hefei*, *Anhui* 230027, *China*

[7] *Key Laboratory of Anhui Province for Emerging and Reemerging Infectious Diseases*, *Hefei*, *Anhui* 230027, *China*

ABSTRACT

Sudan (SUDV) and Bundibugyo (BDBV) ebolaviruses are major outbreak pathogens lacking approved vaccines or therapeutics. Research progress has been hampered by biosafety level 4 (BSL-4) restrictions. Here, we generated recombinant vesicular stomatitis viruses expressing SUDV or BDBV glycoproteins (VSVΔG-SUDV GP, VSVΔG-BDBV GP) and established lethal infection models in Type I interferon receptor knockout (IFNAR$^{-/-}$) mice under BSL-2 conditions. Both surrogate viruses induced rapid, dose-dependent mortality with median lethal dose (LD_{50}) values below 2 PFU. Infected mice developed high viral loads in the liver, spleen, and lungs, along with leukopenia, thrombocytopenia, and elevated transaminases indicating systemic infection and liver injury. Treatment with a single monoclonal antibody rEBOV-515 (mAb 515)) completely protected mice from lethal challenge, reducing viral loads and restoring body weight. These findings establish reproducible surrogate models for studying SUDV and BDBV infection and provide an accessible experimental platform for evaluating GP-targeting therapeutic strategies under BSL-2 conditions.

Keywords: VSV-based surrogate virus; Sudan virus (SUDV); Bundibugyo virus (BDBV); IFNAR$^{-/-}$ mouse model; Animal model

INTRODUCTION

Orthoebolaviruses (genus *Ebolavirus*, family Filoviridae) are highly pathogenic zoonotic viruses that cause severe hemorrhagic fever in humans and non-human primates. Among the species capable of infecting humans are Ebola virus (Zaire ebolavirus), Sudan virus, Bundibugyo virus, and Tai Forest virus, with reported case-fatality rates ranging from 25% to 90%. Among the six known species, Zaire ebolavirus (EBOV) has been the primary cause of large-scale outbreaks in West and Central Africa. The successful development of rVSV-ZEBOV (Ervebo) and licensed monoclonal antibody therapies such as Inmazeb and Ebanga has markedly reduced mortality associated with EBOV infection (Sivanandy et al., 2022). However, Sudan ebolavirus (SUDV) and Bundibugyo ebolavirus (BDBV) continue to cause sporadic but deadly outbreaks in Africa, with no approved vaccines or therapeutics currently available (Languon & Quaye, 2019; Sah et al., 2023). The most recent SUDV outbreak in Uganda in

Received: 03 February 2026; Accepted: 02 March 2026; Online: 15 March 2026

Foundation items: This work was supported by the Strategic Priority Research Program of the Chinese Academy of Sciences (Grant No. XDB0490000), the Wuhan Natural Science Foundation Exploration Program (Grant No. 2024040801020248), the National Natural Science Foundation of China (Grant No. 32400777), the National Key Research and Development Program of China (Grant No. 2024YFC2309400), and the Hubei Provincial Health Commission Science and Technology Project (Grant No. WJ2025M145).

[#]Authors contributed equally to this work

*Corresponding authors, E-mail: qiux@ustc.edu.cn; zhangxh@wh.iov.cn; yanfh1990@163.com

2025 underscored the urgent need for effective countermeasures, with multiple confirmed fatalities. (WHO Disease Outbreak News, 2025 https://www.who.int/emergencies/disease-outbreak-news/item/2025-DON566?)

SUDV and BDBV share many pathogenic features with EBOV but differ significantly in glycoprotein (GP) sequence, antigenicity, and immune evasion mechanisms, rendering EBOV-based vaccines and antibodies only partially protective (Urbanowicz et al., 2016). The lack of safe and practical animal models for these non-Zaire ebolaviruses represents a critical gap in filovirus research. Working with wild-type viruses requires biosafety level-4 (BSL-4) laboratories, which are scarce and costly to operate. This constraint severely limits preclinical evaluation of vaccines and therapeutic antibodies, delaying translational progress.

To overcome this challenge, recombinant vesicular stomatitis virus (VSV)-based platforms have been engineered to express filovirus GPs in place of the native VSV-G, producing replication-competent but attenuated chimeric viruses that can be handled safely under BSL-2 conditions. These surrogate models largely recapitulate the glycoprotein (GP)-mediated entry process of filoviruses, as well as key pathological features of infection, including viremia and damage to vital organs such as the liver and spleen, and have played a crucial role in the development of Ebola virus vaccines and therapeutics (Yang et al., 2024; Zhang et al., 2024; Zhou et al., 2025). However, lethal surrogate models for SUDV and BDBV have not yet been reported, limiting the ability to test broad-spectrum countermeasures.

Wild-type laboratory mice are inherently refractory to productive infection and overt disease following exposure to both authentic ebolaviruses and VSV-based filovirus surrogate viruses. This resistance is predominantly mediated by an intact type I interferon (IFN) signaling pathway, which rapidly induces antiviral gene expression and restricts early viral replication in multiple tissues (Lennemann et al., 2017; Spengler et al., 2023). In contrast, mice lacking the type I interferon receptor ($IFNAR^{-/-}$) are highly susceptible to viral replication and disease due to impaired innate antiviral responses, permitting systemic dissemination and development of clinical signs that more closely resemble filovirus disease in humans (Jiménez-Cabello et al., 2024; Meyts & Casanova, 2021). Consequently, $IFNAR^{-/-}$ mice have been widely adopted in the filovirus field to establish lethal infection models with wild-type or surrogate viruses and to evaluate candidate vaccines and antibody therapies in a controlled, small animal setting. They have been widely used to establish lethal infection models for viruses such as Zika, Marburg virus, Lassa virus and Ebola virus (Lemmens et al., 2023; Marzi et al., 2018; Saito et al., 2020; Siragam et al., 2018; Wang et al., 2024; Wong & Qiu, 2018). Building upon this foundation, we hypothesized that VSV-based surrogates expressing the SUDV or BDBV glycoproteins could produce a robust and lethal phenotype in $IFNAR^{-/-}$ mice, suitable for preclinical evaluation of antivirals and monoclonal antibodies under BSL-2 conditions.

Here, we report the generation and characterization of VSVΔG-SUDV GP and VSVΔG-BDBV GP, and the establishment of the first lethal surrogate models of SUDV and BDBV infection in $IFNAR^{-/-}$ mice. We define their dose-dependent lethality, tissue tropism, and pathophysiological signatures, and demonstrate that treatment with monoclonal antibody rEBOV-515 (mAb 515) provides complete protection from disease. This model recapitulates key pathogenic processes, including systemic viral dissemination, coagulopathy, and hepatic damage, thereby providing a feasible surrogate platform for evaluating vaccines and therapeutics against SUDV and BDBV ebolaviruses.

MATERIALS AND METHOD

Cell lines, Antibodies and Virus construction

Vero E6 cells (CRL-1586, ATCC) and BSR-T7 cells were stored at the Wuhan Institute of Virology, Chinese Academy of Sciences, and cultured in DMEM (Gibco, USA) supplemented with 10% fetal bovine serum (FBS) and 1% penicillin-streptomycin at 37°C with 5% CO_2, with continuous passaging. 293F cells (GDC0655, CCTCC) were cultured in SMM 293-TII expression medium (Sino Biological, China) at 37°C, 130 rpm, 8% CO_2, and 80% humidity.

Monoclonal antibody mAb 515 is a broadly neutralizing human antibody originally isolated from a survivor of Ebola virus disease (EVD) and subsequently engineered to enhance potency and cross-reactivity. It targets a conserved epitope at the base of the Zaire ebolavirus (Makona variant) glycoprotein (GP) trimer that is critical for viral fusion and entry. Structural and functional studies have demonstrated that mAb 515 neutralizes multiple Ebolavirus species by blocking GP conformational rearrangements and mediating Fc-dependent antiviral functions (Gilchuk et al., 2021).

For this study, recombinant mAb 515 was expressed in 293F cells using codon-optimized heavy- and light-chain genes cloned into human IgG1 expression vectors. Culture supernatants were collected 5 days post-transfection and purified by Protein A affinity chromatography resin (GenScript, China) followed by buffer exchange into phosphate-buffered saline (PBS, pH 7.4). Antibody integrity and purity were confirmed by SDS-PAGE and size-exclusion chromatography. The final concentration was adjusted to 5 mg/mL and stored at -80°C until use.

Rescue of recombinant virus

Recombinant plasmid construction and recombinant virus rescue were carried out according to previously described protocol (Wang et al., 2022, 2025). The glycoprotein (GP) coding sequences of Sudan virus (GenBank: NC_006432.1) and Bundibugyo virus (GenBank: MT680253.1) were synthesized and cloned into the pcDNA3.1-VSV-eGFP backbone plasmid, which contains the full-length genome of vesicular stomatitis virus (VSV) Indiana. In these constructs, designated pcDNA3.1-VSVΔG-SUDV GP-eGFP and pcDNA3.1-VSVΔG-BDBV GP-eGFP, the native VSV G gene was replaced with the corresponding filovirus GP gene. Recombinant VSVs were rescued using a reverse genetics system. Briefly, BSR-T7 cells were transfected using the calcium phosphate method (Thermo Fisher, USA) with a mixture of plasmids including 1.25 μg of the full-length VSV plasmid together with support plasmids expressing the VSV N (0.75 μg), P (1.25 μg), L (0.25 μg), and G proteins (2 μg) per well of a 6-well plate according to the manufacturer's instructions (Figure 1A). At 60 hours post-transfection, culture supernatants containing rescued rVSVs were harvested and stored at -80°C. The resulting recombinant viruses were designated VSVΔG-SUDV GP and VSVΔG-BDBV GP, respectively.

Viral characterization

Growth kinetics: Vero E6 cells were infected with VSVΔG-SUDV GP or VSVΔG-BDBV GP at a multiplicity of infection

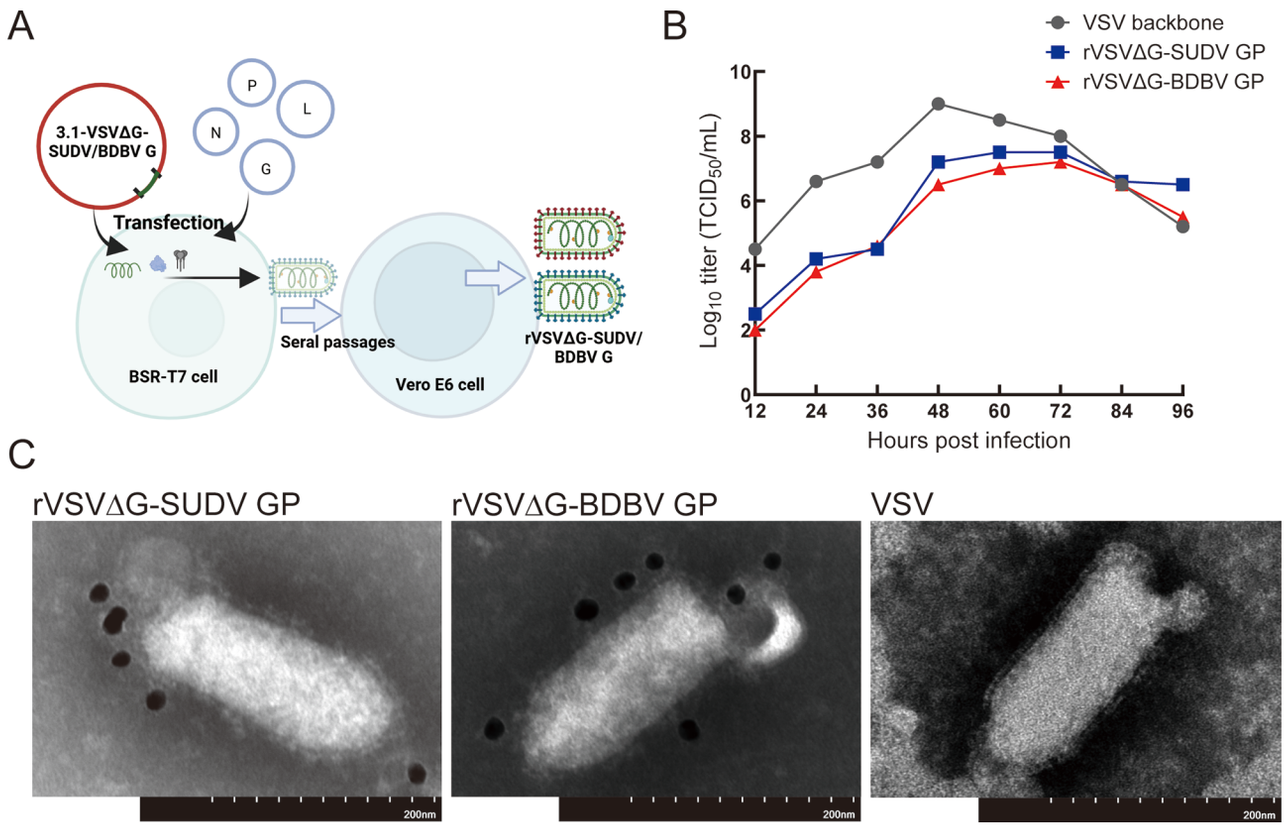

Figure 1 Construction and characterization of recombinant VSV-based surrogate viruses

A: Schematic overview of the rescue strategy for recombinant viruses. Full-length VSV genomes encoding either SUDV GP or BDBV GP (VSVΔG-SUDV GP and VSVΔG-BDBV GP), together with helper plasmids expressing VSV N, P, L, and G proteins, were co-transfected into BSR cells. Supernatants were subsequently passaged on Vero E6 cells to amplify the rescued viruses. B: Growth kinetics of VSVΔG-SUDV GP and VSVΔG-BDBV GP in Vero E6 cells. Cells were infected at an MOI of 0.01, and viral titers at the indicated time points were determined by $TCID_{50}$ assay. C: Immunoelectron microscopy analysis of recombinant virions. VSVΔG-SUDV GP and VSVΔG-BDBV GP exhibited typical rhabdovirus morphology. Surface glycoprotein expression was confirmed by labeling with SUDV or BDBV-specific primary antibodies followed by gold-conjugated secondary antibodies (black dots).

(MOI) of 0.01. Culture supernatants were harvested at designated time points (12, 24, 36, 48, 60, 72, 84, and 96 hours post-infection) and viral titers were quantified by $TCID_{50}$ assay using the Reed–Muench method (Ramakrishnan, 2016).

Immunoelectron microscopy identification: β-propiolactone-inactivated VSV, VSVΔG-SUDV GP, and VSVΔG-BDBV GP preparations were subjected to immunoelectron microscopy. Briefly, 30 μL of each viral suspension was placed onto Parafilm, and Formvar/carbon-coated copper grids were floated on the droplets for 20 minutes at room temperature on a micro-shaker (50 rpm) to allow virion adsorption. After removing excess liquid, grids were fixed with 4% paraformaldehyde for 5 minutes and rinsed once with PBS. Grids were then blocked with 1% skim milk for 1 hour and incubated with the primary antibody 8G6 (Li et al., 2024) targeting SUDV or BDBV GP (1:50 dilution) for 1 hour at room temperature. After three 5-minute washes with PBS, the grids were incubated for 1 hour with a 1:10 dilution of peroxidase-conjugated AffiniPure™ Goat Anti-Mouse IgG (H+L) gold-conjugated secondary antibody (Jackson, China). After two additional PBS washes and three distilled water rinses, grids were negatively stained with 2% uranyl acetate for 2 minutes, blotted, and air-dried. Samples were examined using a transmission electron microscope operated at 80 kV. Throughout the procedure, grids were handled only at the outer edge to avoid damaging the support film, and moisture was maintained during transfers to preserve virion integrity.

Virus titration assay: Vero E6 cells were seeded into 24-well plates at a density of 2×10^5 cells/mL (500 μL per well) and incubated overnight at 37°C with 5% CO_2. The recombinant viruses VSVΔG-SUDV GP and VSVΔG-BDBV GP were serially diluted in 10-fold increments across eight dilutions starting from 10^{-1}. A 100 μL aliquot of each dilution was inoculated onto the Vero E6 monolayer, with uninfected wells serving as negative controls. After 1 h of adsorption, the inoculum was removed and replaced with DMEM supplemented with 2% FBS, 1% penicillin–streptomycin, and 1% methylcellulose. Plates were incubated at 37°C with 5% CO_2 for 2–3 days. Cells were then fixed with 10% neutral-buffered formalin and stained with 1% crystal violet. Viral titers were calculated according to the formula:

$$\text{Virus titer (PFU/mL)} = \text{Mean Plaque Count} \times \text{Dilution Factor} \times 10$$

Animal experiments

Ethics statement: All animal experiments conformed to the standards for use and care of laboratory animals and were approved by the Institutional Review Board of the Wuhan Institute of Virology, Chinese Academy of Sciences (approval number: WIVA45202311). 6–8 week-old female and male C57BL/6JGpt mice (strain number: T005534) were used in this study. These mice, which are deficient in the type I interferon receptor, were bred and maintained under specific

pathogen-free (SPF) conditions in our animal facility.

LD_{50} determination: For the LD_{50} determination experiment, female and male mice were divided into five groups for each virus (VSVΔG-SUDV GP and VSVΔG-BDBV GP), with three mice per group. Mice were inoculated intraperitoneally (i.p.) with 100 μL of serially diluted virus stock, ranging from 10^4 to 10^0 PFU/mL. Body weight and survival rates were recorded daily. A humane endpoint was defined as a reduction in body weight to below 75% of the original body weight.

Establishment of systemic infection and pathological models: To evaluate systemic infection and pathological symptoms induced by the virus, 6–8 week-old female IFNAR$^{-/-}$ mice were divided into three groups: two virus-infected groups (n=6) and control group (n=6). Infected groups received an i.p. injection of 100 μL containing 85.8 and 55.0 PFU/mL (approximately 10 LD_{50}) of the respective surrogate virus, while the control group received an equal volume of DMEM via the same route. Three days post-infection, blood samples were collected via the retro-orbital plexus for complete blood count and blood biochemical analysis. To assess systemic viral dissemination, heart, liver, spleen, lungs, kidneys, and brain samples were collected for pathological examination and viral distribution analysis.

Evaluation of antibody efficacy: To assess the suitability of this model for antibody evaluation, 6–8 week-old female IFNAR$^{-/-}$ mice were divided into five groups (n=8 per group). Four of these were experimental groups receiving an i.p. injection of 100 μL containing 85.8 and 55.0 PFU/mL (approximately 10 LD_{50}) of the surrogate virus. Two of the experimented groups received an i.p. injection of 10 mg/kg monoclonal antibody 515 (100 μL per mouse) one day post-challenge. One control group received an equal volume of DMEM followed by an equal volume of PBS one day post-challenge. On the third day post-infection, three mice randomly selected from each group were euthanized. Tissue samples including heart, liver, spleen, lungs, kidneys, and brain were collected for viral titer determination and pathological analysis. The remaining mice were continuously monitored for changes in body weight and survival rates.

Sample detection and analysis

Treatment of tissue samples: Collected tissues were placed into sterile grinding tubes containing 1 mL of DMEM supplemented with 1% penicillin–streptomycin. Samples were homogenized using a tissue homogenizer (LanHen Biotechnology, China) under the following program: 30 s run, 15 s pause, frequency 60 Hz. Homogenates were centrifuged at 10 000 × *g* for 15 min at 4°C to remove debris, and supernatants were collected for subsequent analysis.

RT-qPCR: A 300 μL aliquot of each tissue supernatant was used for viral RNA extraction with the VAMNE Virus DNA/RNA Extraction Kit 3.0 (Vazyme, China). Quantification of viral RNA was performed using the HiScript II One Step qRT-PCR SYBR Green Kit (Vazyme, China) following the manufacturer's protocol. The following primer pairs were used to amplify the VSV N gene:

Forward primer (VSV-N F): 5′-TGATCGACTTTGGATTGTCTTCTAA-3′

Reverse primer (VSV-N R): 5′-TCTGGTGGATCTGAGCAGAAGAG-3′

The cycling parameters were: reverse transcription at 50°C for 3 min, initial denaturation at 95°C for 30 s, followed by 40 cycles of 95°C for 10 s and 60°C for 30 s. A melting-curve analysis was performed from 65°C to 95°C, increasing by 0.5°C every 5 s. Viral RNA copy numbers were calculated using a standard curve generated from serially diluted in-vitro-transcribed RNA.

$TCID_{50}$ assay: Vero E6 cells were seeded into 96-well plates at a density of 2 × 10^5 cells mL^{-1} (100 μL per well) and incubated overnight at 37°C with 5%CO_2 until 80–90% confluent. Tissue supernatants were serially diluted 10-fold (10^{-1} to 10^{-6}), and 100 μL of each dilution was added to replicate wells. After 3 days of incubation, wells were examined microscopically for cytopathic effect (CPE). The median tissue-culture infectious dose ($TCID_{50}$) mL^{-1} was determined using the Reed-Muench method.

Hematology and biochemical analysis: Whole blood was collected from anesthetized mice via the retro-orbital plexus into EDTA-K_2 anticoagulant tubes. Complete blood counts were performed using an automated hematology analyzer (HEMAVET® 950FS, Drew Scientific, USA) according to the manufacturer's instructions. Parameters measured included total white blood cell (WBC) count, lymphocyte percentage (LYM%), granulocyte percentage (GRAN%), platelet count (PLT), and red blood cell (RBC) indices.

Histopathology and Immunohistochemistry: Tissue samples, including liver, spleen, lung, kidney, and brain, were fixed in 10% neutral-buffered formalin for at least 48 h and embedded in paraffin. Sections (5 μm thickness) were prepared and stained with hematoxylin and eosin (H&E) following standard protocols.

For immunohistochemical (IHC) staining, sections were deparaffinized, rehydrated, and subjected to antigen retrieval using citrate buffer (pH 6.0). Endogenous peroxidase activity was quenched with 3% hydrogen peroxide for 10 min. After blocking with 5% bovine serum albumin (BSA), the sections were incubated overnight at 4°C with a primary human monoclonal antibody FVM04 (prepared in-house) specific for SUDV and BDBV GP. Detection was performed using an HRP-conjugated goat anti-human IgG secondary antibody (ABclonal, China) and visualized with diaminobenzidine (DAB) substrate.

Histopathological evaluation was performed according to the INHAND (International Harmonization of Nomenclature and Diagnostic Criteria for Lesions in Rats and Mice) guidelines. Semi-quantitative pathological scores were assigned independently by two blinded pathologists based on the severity and distribution of lesions.

Statistical analysis

All data were analyzed using GraphPad Prism v.10.0 (GraphPad Software, USA). Results are presented as mean ± standard error of the mean (SEM). For comparisons between two experimental groups, statistical significance was determined using an unpaired Student's *t*-test. When more than two experimental groups were compared, one-way analysis of variance (ANOVA) was employed, as specified in the figure legends. *P*-values less than 0.05 were considered statistically significant and are indicated as follows: *: $p<0.05$; **: $p<0.01$; ***: $p<0.001$; ****: $p<0.0001$; ns: Not significant.

RESULTS

The recombinant surrogate viruses were successfully rescued and characterized

The recombinant viruses VSVΔG-SUDV GP and VSVΔG-BDBV GP were successfully rescued and confirmed through growth kinetics analysis and immunoelectron microscopy

(Figure 1B, C). Growth curve analysis demonstrated that both recombinant viruses replicated efficiently in Vero E6 cells, exhibiting comparable kinetics. Peak titers reached approximately $10^{7.5}$ and $10^{7.2}$ $TCID_{50}$/mL for VSVΔG-SUDV GP and VSVΔG-BDBV GP, respectively, at 72 hours post-infection (Figure 1B). To further verify virion morphology and the incorporation of the heterologous filovirus glycoproteins, immunoelectron microscopy was performed. Both recombinant viruses exhibited the characteristic bullet-shaped morphology of Rhabdoviridae: an enveloped particle approximately 180 nm in length and 50–70 nm in diameter, containing a dense helical nucleocapsid consistent with typical VSV ultrastructure (Figure 1C). No detectable structural abnormalities were observed relative to the parental VSV. Specific labeling of the surface glycoproteins was confirmed following incubation with SUDV or BDBV glycoprotein specific primary antibodies and gold-conjugated secondary antibodies. Distinct approximately 18 nm colloidal gold particles were observed decorating the viral envelope of VSVΔG-SUDV GP and VSVΔG-BDBV GP, whereas no gold labeling was present on the parental VSV control (Figure 1C). This result confirms successful incorporation and surface presentation of SUDV and BDBV glycoproteins on the recombinant virions. Collectively, these findings demonstrate that the VSVΔG-SUDV GP and VSVΔG-BDBV GP viruses were efficiently rescued and retain typical rhabdovirus morphology while displaying the appropriate exogenous filovirus glycoproteins on their surface.

Lethality and LD_{50} determination of VSVΔG-SUDV GP and VSVΔG-BDBV GP in IFNAR$^{-/-}$ mice

To determine the median lethal dose (LD_{50}) of recombinant VSV surrogates, groups of IFNAR$^{-/-}$ mice were inoculated intraperitoneally (i.p.) with serial 10-fold dilutions ranging from 10^3 to 10^{-1} PFU per animal. Daily monitoring of body weight and survival revealed clear, dose-dependent lethality for both VSVΔG-SUDV GP and VSVΔG-BDBV GP.

In the VSVΔG-SUDV GP-infected cohort, IFNAR$^{-/-}$ mice receiving 10^0 PFU exhibited mild weight loss (10.5% relative to day 0 at day 8 post infection) and a survival rate of 50% at the experimental endpoint, whereas lower doses caused no mortality or significant weight change. Higher doses (10^1–10^3 PFU) induced uniform lethality within 2–6 days (Figure 2A, B). Similar body weight changes, survival rates, and LD_{50} values below 2 PFU were observed in both female and male mice, with no significant differences noted between sexes (Supplementary Figure S1A, B).

For VSVΔG-BDBV GP, IFNAR$^{-/-}$ mice challenged with 10^0 PFU displayed a 9% weight reduction by day 5 and a survival rate of 50%, whereas the 10^{-1} PFU group showed only minor weight loss and 83.3% survival. High-dose infection again caused complete lethality within 4–7 days (Figure 2C, D). Following challenge with VSV-BDBV GP, similar pathogenicity was observed in both female and male mice, with no marked sex-based differences noted (Supplementary Figure 1C, D).

Using probit analysis, the LD_{50} values of VSVΔG-SUDV GP were estimated as 1.027 PFU (Figure 2B), with 0.858 PFU for female and 1.437 PFU for male respectively (Supplementary Figure S1A, B). For VSVΔG-BDBV GP group, the LD_{50} values were estimated as 1.000 PFU (Figure 2D), with 0.550 PFU for female and 1.437 PFU for male respectively (Supplementary Figure S1C, D). These findings demonstrate that both surrogate viruses establish highly lethal infections in IFNAR$^{-/-}$ mice, with extremely low LD_{50} values consistent with systemic susceptibility in the absence of type I interferon signaling.

Systemic viral replication and pathology induced by VSVΔG-SUDV GP and VSVΔG-BDBV GP in IFNAR$^{-/-}$ mice

To characterize the pathogenicity of the surrogate viruses, groups of female IFNAR$^{-/-}$ mice (n=5 per group) were intraperitoneally challenged with 10 LD_{50} of either VSVΔG-SUDV GP or VSVΔG-BDBV GP, while control animals received DMEM. At 3 days post infection (dpi), mice were euthanized, and blood as well as major organs including the heart, liver, spleen, lung, kidney, and brain were collected for analysis (Figure 3A).

Quantitative assessment of viral RNA and infectious titers demonstrated systemic dissemination of both surrogate viruses, with significantly higher levels than those in mock-infected animals. Viral replication was most pronounced in the liver, spleen, and lungs, where RNA levels reached $10^{9.6}$, $10^{9.8}$, and $10^{9.4}$ copies per gram of tissue respectively for VSVΔG-SUDV GP, and $10^{8.4}$, $10^{7.5}$, and $10^{8.1}$ copies per gram of tissue respectively for VSVΔG-BDBV GP (Figure 3B). Corresponding infectious titers reached up to $10^{6.5}$, $10^{6.9}$, and $10^{5.7}$ $TCID_{50}$/g of tissue (liver, spleen, and lung, respectively) for VSVΔG-SUDV GP, and $10^{4.2}$, $10^{4.4}$, and $10^{3.7}$ $TCID_{50}$/g of tissue (also respectively) for VSVΔG-BDBV GP (Figure 3C). These findings indicate that both surrogate viruses preferentially replicate in the liver, spleen, and lungs which are the principal target organs for Ebolavirus infection.

Histopathological examination of the liver, spleen, lung, and kidney at 3 dpi revealed multifocal organ damage, with the most severe lesions observed in the liver. Hepatic pathology was characterized by extensive hepatocyte necrosis (orange arrows) exhibiting pyknosis, karyorrhexis, and karyolysis, widespread vacuolar degeneration (yellow arrows), mild fibroblast proliferation (brown arrows) within hepatic sinusoids, and marked venous and sinusoidal congestion (green arrows). The spleen displayed abundant necrotic debris within the white pulp (yellow arrows), mild granulocyte infiltration in the red pulp (cyan arrows), and pronounced sinusoidal dilation (green arrows). Pulmonary sections revealed moderate alveolar wall thickening, interstitial edema, pronounced granulocyte infiltration (cyan arrows), and perivascular hemorrhage (green arrows). In the kidneys, mild tubular epithelial cell edema (blue arrows) and vacuolar degeneration (yellow arrows) were evident. The brain tissue contained a rich number of neurons. A small number of shrunken nerve cells were visible in the cortex, and a small number of shrunken granular cells were observed in the hippocampal DG region (yellow arrow). (Figure 3E; Supplementary Figure S2). Quantitative pathology scoring confirmed that the liver sustained the highest degree of tissue injury (Figure 3D). Similarly, immunohistochemical results demonstrated the presence of viral antigens was clearly observed in the liver and spleen tissues of infected mice, whereas this phenomenon was less pronounced in the lungs and kidneys. No viral antigens were detected in the brain tissue (Figure 3F).

Hematological analyses further demonstrated systemic involvement. Infected mice showed increased neutrophil percentages (GRAN%), markedly reduced platelet counts (PLT), and decreased lymphocyte percentages (LYM%) and lymphocyte counts (LYM), indicative of coagulation abnormalities and immune dysregulation. Total white blood cell (WBC) counts were also significantly reduced, consistent with leukocyte depletion (Figure 4A–D; Supplementary Figure 3B). Although Hematological analysis revealed a

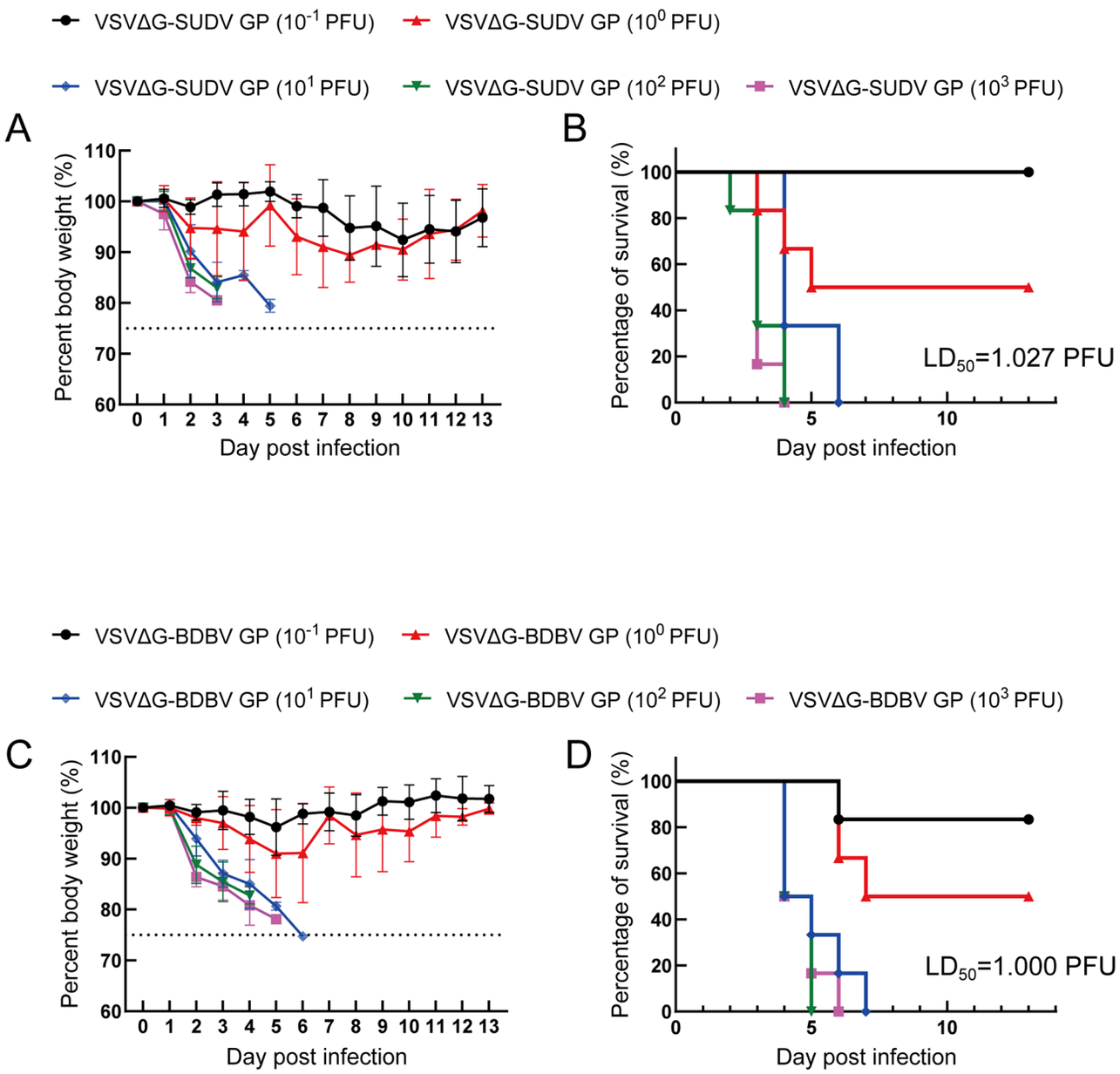

Figure 2 Lethality and median lethal dose (LD_{50}) determination of VSVΔG-SUDV GP and VSVΔG-BDBV GP

A, B: Body weight changes (A) and survival (B) of IFNAR$^{-/-}$ mice inoculated intraperitoneally (i.p.) with different doses of VSVΔG-SUDV GP (n=6 per group). C, D: Body weight changes (C) and survival (D) of IFNAR$^{-/-}$ mice inoculated with different doses of VSVΔG-BDBV GP (n=6 per group). LD_{50} values were calculated by IBM SPSS Statistics (Version 27).

relative increase in the percentage of neutrophils, their absolute count showed no significant difference compared to the control group (Supplementary Figure 3A). This pattern suggests severe leukopenia accompanied by a relative neutrophilic inflammatory response. Serum biochemical profiling corroborated the evidence of hepatic injury. Alanine aminotransferase (ALT) and aspartate aminotransferase (AST) levels were markedly elevated (Figure 4E, F), while alkaline phosphatase (ALP) levels moderately declined (Figure 4H), reflecting hepatic dysfunction. Serum albumin concentrations remained unchanged relative to controls (Figure 4G).

Collectively, these data demonstrate that VSVΔG-SUDV GP and VSVΔG-BDBV GP establish systemic, multi-organ infection in IFNAR$^{-/-}$ mice, accompanied by severe hepatic injury, hematological abnormalities, and dysregulation of liver enzymes. While the present study does not aim to attribute these pathological manifestations exclusively to filovirus glycoprotein-specific effects, the overall disease course—including viral dissemination patterns, target organ involvement, and host injury profiles—exhibits several core pathological features similar to those observed during authentic Ebolavirus infection. These findings support the utility of VSV-based surrogate viruses in IFNAR$^{-/-}$ mice as physiologically relevant and experimentally accessible models for preclinical evaluation of vaccines and antibody-based therapeutics under BSL-2 conditions.

Monoclonal antibody treatment confers complete protection against lethal VSVΔG-SUDV GP and VSVΔG-BDBV GP infection

To further validate the robustness of the lethal surrogate models, female IFNAR$^{-/-}$ mice were intraperitoneally challenged with 10 LD_{50} of either VSVΔG-SUDV GP or VSVΔG-BDBV GP. At 1 day post infection (dpi), animals

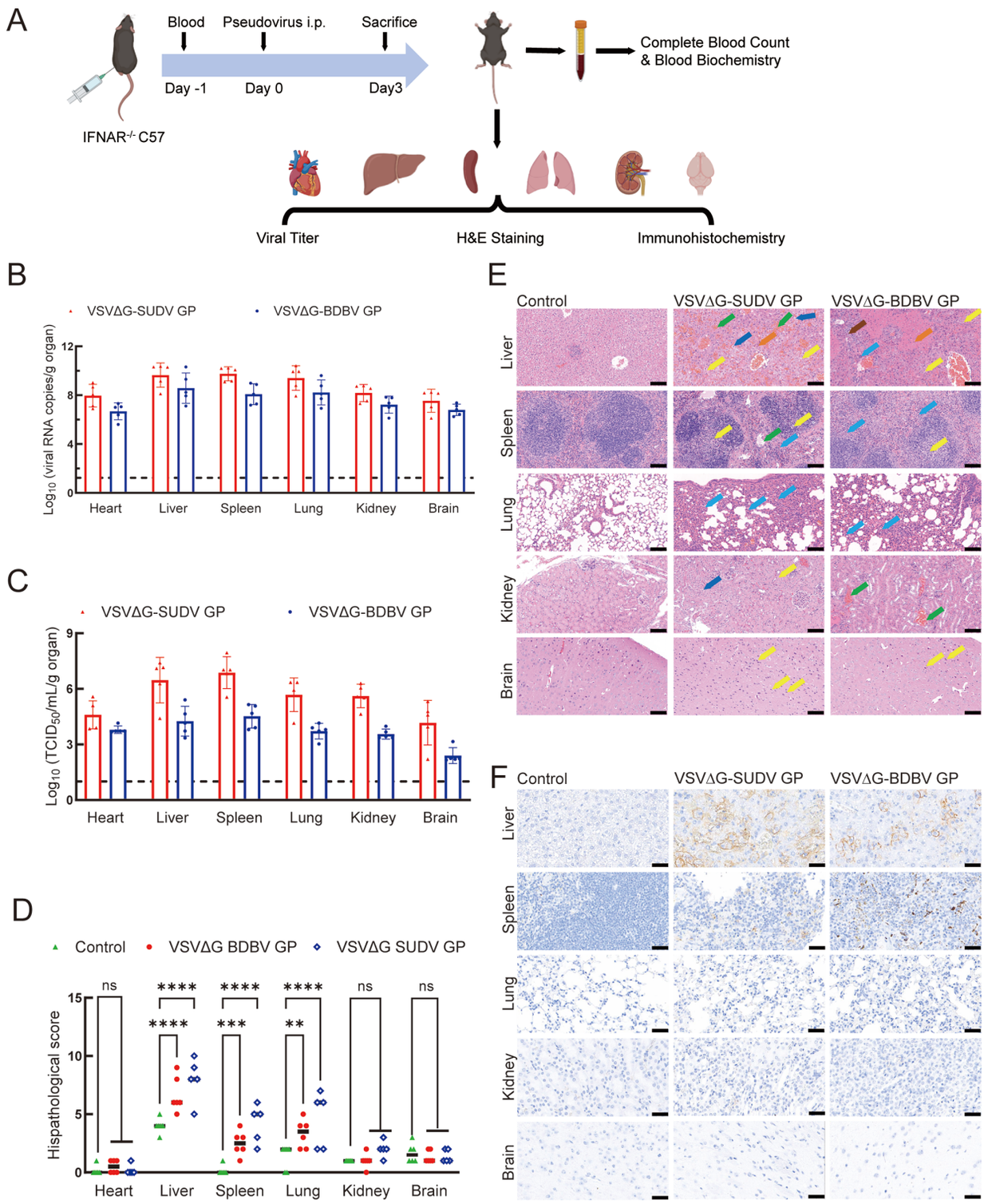

Figure 3 Viral dissemination and organ tropism at day 3 post-infection

A: Schematic of the experimental design: IFNAR$^{-/-}$ mice were inoculated i.p. with 10 LD_{50} of VSVΔG-SUDV GP or VSVΔG-BDBV GP (n=5 per group). On day 3 post-infection, blood and tissues (heart, liver, spleen, lungs, kidneys, brain) were collected. Blood was analyzed for complete blood count and biochemistry, and tissues were used to assess viral distribution and pathology. B: Viral RNA copies numbers in various organs of VSVΔG-SUDV GP group and VSVΔG-BDBV GP group. C: Live virus titers in various organs of VSVΔG-BDBV GP group and VSVΔG-BDBV GP group. D: Quantification of pathological scores. ns: Not significant; *: P<0.05; **: P<0.01; ***: P<0.001; ****: P<0.0001. E: Representative H&E-stained tissue sections (magnification, 20×; scale bar, 100 μm) showing virus-induced lesions. Hepatic lesions including vein congestion (green arrows), vacuolar degeneration (yellow arrows), focal necrosis of hepatocytes (orange arrows), lymphocytic infiltration (light blue arrows) and hepatic sinusoidal fibrosis (brown arrows) were observed. Splenic lesions consisting of sinusoidal dilation (green arrows), Necrotic debris in the white pulp (yellow arrows) and neutrophilic infiltrate (light blue arrow) were exhibited. Pulmonary lesions including neutrophilic infiltration (light blue arrow) were marked. Kidney lesions containing vein congestion (green arrows), vacuolar degeneration (yellow arrows) and cellular swelling (blue arrows) were labelled. Brain lesions such as neuronal shrinkage were marked by yellow arrows. F: Immunohistochemical (magnification, 20×; scale bar, 100 μm) results demonstrated the presence of viral antigen in liver and spleen. Positive immunoreactivity (brown signal) is observed.

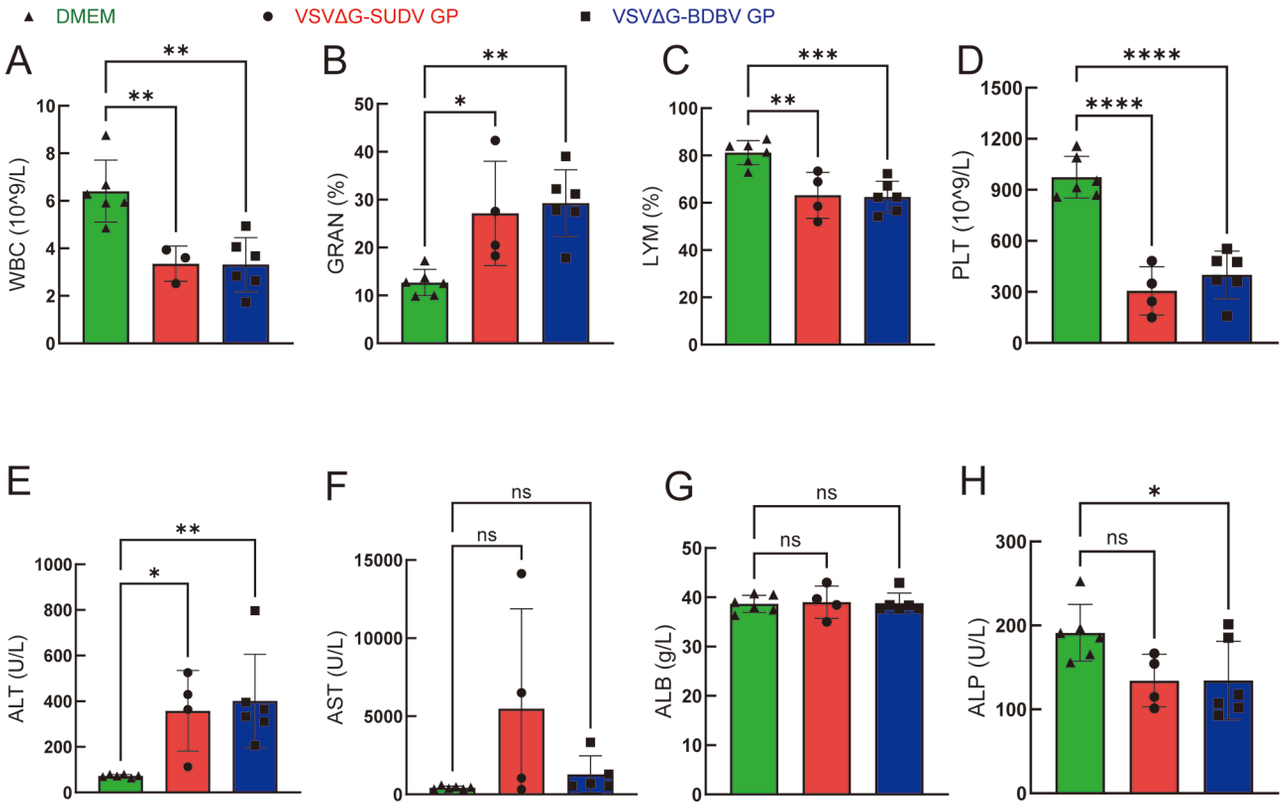

Figure 4 Hematological and biochemical abnormalities in infected mice

Complete blood count analysis at three day-post-infection, A: white blood cell counts (WBC), B: neutrophil percentages (GRAN%), C: lymphocyte percentages (LYM%) and D: Platelet counts (PLT). Blood biochemistry analysis included E: alanine aminotransferase (ALT), F: aspartate aminotransferase (AST), G: albumin (ALB), and G: alkaline phosphatase (ALP). ns: Not significant; *: P<0.05; **: P<0.01; ***: P<0.001; ****: P<0.0001.

received intraperitoneal administration of monoclonal antibody 515 (10 mg/kg), whereas control groups received either an equivalent volume of DMEM (vehicle). Body weight and survival were monitored daily, and a subset of animals was euthanized at 3 dpi for virological and histopathological analyses (Figure 5A).

In the VSVΔG-SUDV GP cohort, untreated mice exhibited rapid and sustained weight loss, succumbing by day 4 post infection. In contrast, antibody-treated animals showed transient weight reduction followed by full recovery, resulting in 100% survival (Figure 5B). Similarly, infection with VSVΔG-BDBV GP induced progressive weight loss beginning at day 2, with complete mortality by day 7 in untreated controls. Administration of mAb 515 markedly attenuated weight loss and conferred complete protection, with all treated mice surviving to the study endpoint (Figure 5C, D).

Quantitative analysis of viral burden in major organs revealed that antibody treatment prevented an increase in both viral RNA copies and infectious titers. In VSVΔG-SUDV GP infected mice, mAb 515 reduced viral RNA loads by approximately $10^{4.4}$ copies/g in the liver and $10^{4.2}$ copies/g in the lungs, while decreasing live virus titers by roughly $10^{3.4}$ $TCID_{50}$/g in the liver. Similarly, in VSVΔG-BDBV GP infected mice, treatment led to reductions of $10^{3.8}$ copies/g in the liver and $10^{2.8}$ copies/g in the spleen, with corresponding decreases of $10^{1.6}$ $TCID_{50}$/g in liver tissue but no significant differences were observed in the brain tissue (Figure 5E–H). These results indicate that mAb 515 prevents or significantly restricts viral dissemination in target organs, effectively curbing viral dissemination and disease progression in $IFNAR^{-/-}$ mice.

Histopathological examination and immunohistochemical analysis revealed that treatment with the monoclonal antibody 515 following VSVΔG-SUDV GP challenge significantly mitigated tissue damage. Specifically, in the liver, there was a marked reduction in focal hepatocyte necrosis and vascular congestion, accompanied by the clearance of viral antigens. In the spleen, dilation of the splenic sinuses was diminished, and viral antigens were cleared from the white pulp. Pathological changes in other organs were also alleviated, including reduced thickening of alveolar walls and septa in the lungs, and the resolution of renal tubular epithelial edema in the kidneys. Notably, viral antigens were effectively cleared from both lung and kidney tissues (Figure 5I, J). A similar therapeutic effect characterized by attenuated inflammation and viral clearance was observed in the VSVΔG-BDBV GP challenge model following antibody 515 treatment (Supplementary Figure 2A, B). Collectively, these results demonstrate that monoclonal antibody 515 effectively ameliorates histopathological lesions and clears viral antigens in infected mice. Furthermore, they support the use of interferon-deficient mice as a viable model for evaluating the protective efficacy of therapeutic antibodies against surrogate virus challenges.

Together, these findings demonstrate that mAb 515 provides complete protection against lethal VSVΔG-SUDV GP and VSVΔG-BDBV GP challenge. The robust therapeutic efficacy observed supports the utility of these $IFNAR^{-/-}$ surrogate models as a practical platform for preclinical evaluation of countermeasures targeting Sudan and Bundibugyo ebolaviruses.

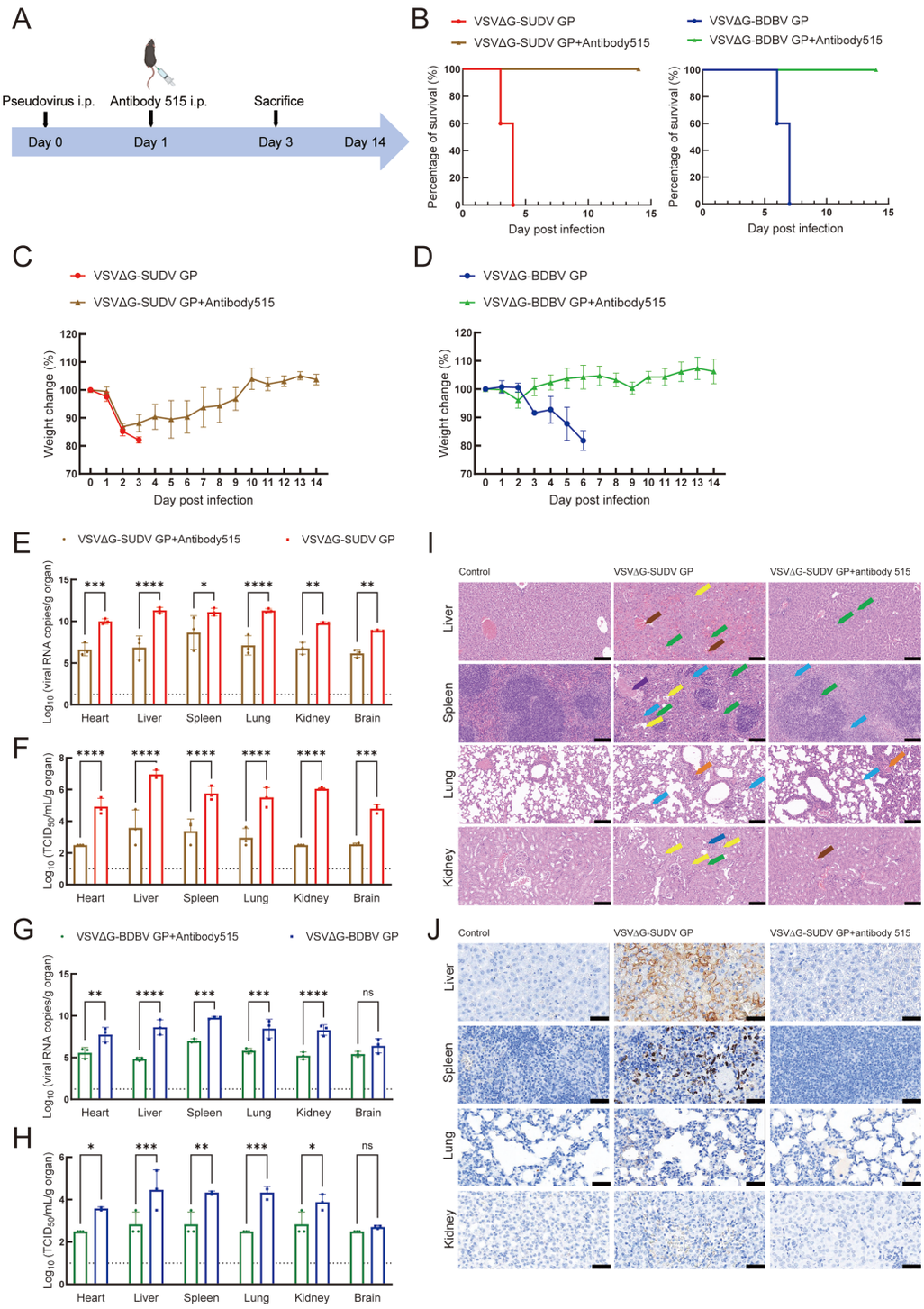

Figure 5 Evaluation of therapeutic efficacy of monoclonal antibody mAb 515

A: Experimental design: IFNAR$^{-/-}$ female mice were divided into five groups. The experimental four groups were challenged i.p. with 10 LD_{50} of VSVΔG-SUDV GP or VSVΔG-BDBV GP respectively and the control group received the same dose of DMEM (n=8 per group). Two of experimental groups were treated i.p. with 10 mg/kg mAb 515 one day post-infection. On day 3 post-challenge, three mice per group were euthanized for tissue collection; remaining mice were monitored for survival. B: Survival rates. C, D: Body weight changes. E, F: Viral RNA copies (E) and live virus titers (F) in various tissues of VSVΔG-SUDV GP. G, H: Viral RNA copies (G) and live virus titers (H) in various tissues of VSVΔG-BDBV GP. ns: Not significant; *: P<0.05; **: P<0.01; ***: P<0.001; ****: P<0.0001. I: H&E staining revealed that mAb 515 attenuated virus-induced tissue lesions. Hepatic lesions including Focal hepatocyte necrosis (green arrow), hepatocyte edema (yellow arrow), and vascular congestion (brown arrow) were observed. Splenic lesions consisting of Splenic sinus dilatation (yellow arrow), granulocyte infiltration (light blue arrow), necrotic cellular debris (green arrow), and insoluble fibrin (purple arrow) were exhibited. Pulmonary lesions including Eosinophilic material is visible within the bronchiolar lumen (orange arrow), accompanied by granulocyte infiltration (light blue arrow) were marked. Kidney lesions containing Renal tubular lumina are filled with eosinophilic material (green arrow), accompanied by cellular edema (yellow arrow), mesangial matrix hyperplasia in the glomerulus (blue arrow), and vascular congestion (brown arrow) were labelled. J: Immunohistochemistry confirmed a decrease in tissue viral load (magnification, 20×; scale bar, 100 μm). Positive immunoreactivity (brown signal) is observed.

DISCUSSION

In this study, we established the first lethal mouse models for Sudan virus (SUDV) and Bundibugyo virus (BDBV) infection using vesicular stomatitis virus (VSV)-based surrogates in IFNAR$^{-/-}$ mice. These models exhibited key features similar to those observed in filovirus disease, including systemic viral dissemination, hematological dysregulation, and severe hepatic injury. Complete protection achieved through monoclonal antibody (mAb) 515 treatment further demonstrates the utility of this platform for preclinical therapeutic evaluation.

Our findings show that VSVΔG-SUDV GP and VSVΔG-BDBV GP infections in IFNAR$^{-/-}$ mice induce an acute and fatal disease course with several features resembling those reported in filovirus infection, including systemic viral dissemination and organ-associated pathology. The dose-dependent lethality observed in these models is comparable to that reported in EBOV surrogate systems (Yang et al., 2024; Zhang et al., 2024), indicating a shared dependency on the susceptible IFNAR$^{-/-}$ host and the replicative VSV backbone. However, this work introduces distinct novelty by providing the first systematic characterization of lethal systemic infection mediated specifically by SUDV and BDBV glycoproteins in a small animal model, thereby addressing a critical methodological gap for these pathogens. Importantly, these surrogates reproduced the multi-organ viral dissemination pattern typical of human Ebola virus disease (EVD), with viral loads peaking in the liver, spleen, and lungs that organs known to support high-level viral replication and to drive the systemic inflammatory and coagulopathic responses associated with fatal outcomes (Bradfute et al., 2010; Martines et al., 2015; Mcelroy et al., 2014).

Beyond replicating systemic infection, our surrogate models captured the dynamic hematological changes characteristic of filovirus pathogenesis. Early in infection, we observed marked leukopenia dominated by lymphocytopenia and transient granulocytosis, closely resembling clinical features of EVD patients (Formenty et al., 1999; Sanchez et al., 2004). As infection progressed, total leukocyte counts rebounded and exceeded baseline levels, accompanied by an increased proportion of immature granulocytes and signs of lymphocyte activation. This biphasic leukocyte response suggests an initial immune suppression phase followed by emergency myelopoiesis and dysregulated activation, which is consistent with the “cytokine storm” and immune exhaustion described in severe Ebola infections. In some fatal cases, leukocyte depletion reemerged, likely reflecting virus-induced destruction of lymphoid architecture in the spleen and lymph nodes (Bradfute et al., 2007; Geisbert et al., 2003). Such oscillating hematologic profiles reinforce the capacity of the IFNAR$^{-/-}$ model to recapitulate immune dysfunction dynamics during filovirus infection. We acknowledge that a detailed characterization of cytokine profiles or GP-specific adaptive immune signatures was not conducted. Future studies utilizing this platform, particularly in the context of vaccine or therapeutic evaluation, could productively incorporate cytokine profiling and analyses of GP-specific humoral or cellular immune responses to further delineate its immunological fidelity to authentic SUDV/BDBV infection.

A particularly noteworthy observation was the biochemical signature of hepatic dysfunction. Under typical viral hepatitis or toxin-induced injury, serum alkaline phosphatase (ALP) levels rise alongside transaminases due to biliary epithelial stress and compensatory proliferation. However, in our interferon-deficient models, ALP levels exhibited only mild or absent elevation despite severe hepatic necrosis and massively increased ALT and AST. We propose that this discordance reflects the rapid, catastrophic destruction of hepatocytes and cholangiocytes before ALP synthesis can be upregulated. This pattern, characterized by disproportionately elevated transaminases and reduced ALP, may serve as a biochemical hallmark of fulminant hepatic necrosis under interferon-deficient conditions (Iluz-Freundlich et al., 2021). Future comparative studies using wild-type and interferon-receptor knockout mice may further elucidate how interferon signaling modulates hepatic regeneration and enzyme release during systemic viral infection.

Another critical insight from this study lies in the therapeutic validation of the models. Administration of monoclonal antibody 515 conferred complete protection against both SUDV and BDBV surrogate infections, as evidenced by full survival, recovery of body weight, and significant reduction of viral RNA and infectious titers in key organs. These findings underscore the value of the model for preclinical screening of neutralizing antibodies and small-molecule antivirals. Importantly, they also provide a proof-of-concept that cross-protective antibodies targeting conserved epitopes within the GP of non-Zaire ebolaviruses can confer potent in vivo efficacy. Such cross-lineage protection suggests the potential utility of GP-targeting strategies across antigenically distinct ebolavirus species, although further validation in authentic virus systems is required.

From a biosafety and translational perspective, the greatest advantage of these VSV-based models is their compatibility with biosafety level 2 (BSL-2) containment. Meanwhile, the recombinant viruses lack the native VSV-G gene, rely exclusively on heterologous filovirus GP for entry, and were passaged under controlled conditions without evidence of reversion. We also emphasize that similar VSV-ΔG platforms have been widely used under BSL-2 containment and are considered genetically stable when properly handled (Dong et al., 2019; Hicks et al., 2024; Yang et al., 2024). This accessibility allows laboratories worldwide to perform mechanistic and therapeutic studies that would otherwise require rare and highly restricted BSL-4 facilities. The availability of BSL-2–compatible lethal models support expanded research into non-Zaire ebolaviruses, facilitate comparative immunopathogenesis studies across species, and accelerate early-stage screening of vaccines and monoclonal antibodies. These models provide a small-animal experimental system that enables controlled studies of infection and therapeutic evaluation in a BSL-2 setting.

While the VSV-based surrogate system in IFNAR$^{-/-}$ mice enables robust and lethal infection under BSL-2 conditions, several limitations should be acknowledged. As previously demonstrated, the substitution of heterologous glycoproteins on the VSV backbone can elicit distinct lethal pathologies in interferon-deficient mice (Dong et al., 2019; Emanuel et al., 2018; Hicks et al., 2024; Yang et al., 2024). We therefore propose that, within this highly susceptible host context, disease severity and histopathological alterations are driven primarily by the specific cytopathic effects mediated by the foreign glycoprotein (GP), rather than resulting solely from uncontrolled VSV replication due to impaired type I interferon signaling. However, although the observed histopathological lesions are biologically relevant and virus-dependent, the current study does not aim to attribute organ damage

exclusively to filovirus GP in the absence of a VSV-G pseudotyped control. This model is therefore optimally positioned as a platform for therapeutic evaluation rather than for dissecting GP-specific mechanisms of tissue injury. Additionally, the remarkably low LD_{50} values may reflect the extreme sensitivity of IFNAR$^{-/-}$ mice combined with potential differences between in vitro plaque assays and actual in vivo infectivity; thus, reported titers should be interpreted as relative measures of biological activity. Other limitations include the lack of assessment of viral persistence in immune-privileged sites like the testes, and the observed discrepancy in the brain (viral RNA detection without antigen) likely reflects low-level or non-productive infection limited by the blood-brain barrier and cell-intrinsic defenses, where protein expression falls below the detection threshold of immunohistochemistry, and the sex-based differences warrant further investigation in future studies with larger cohort sizes.

Importantly, the complete protection conferred by mAb-515, including survival benefit, profound reduction of viral loads, and marked attenuation of tissue injury, supports the utility of this model as a sensitive and reproducible platform for evaluating neutralizing antibodies and antiviral countermeasures against SUDV and BDBV. Previous studies have shown that VSV-G can induce high viremia, multi-organ involvement, and severe pathology in IFNAR$^{-/-}$ mice, although tissue tropism and the extent of organ-specific injury may vary depending on viral dose, route of inoculation, and experimental timing (Fang et al., 2012; Meyts & Casanova, 2021; Mishra et al., 2020).

Future studies incorporating additional viral controls will be valuable for further dissecting GP-specific contributions to pathogenesis; however, such analyses fall outside the primary scope of the present work, which focuses on preclinical efficacy assessment under accessible biosafety conditions.

Collectively, our work establishes a reproducible, safe, and mechanistically relevant surrogate system for studying SUDV and BDBV pathogenesis and evaluating candidate therapeutics. By bridging the gap between cell culture assays and high-containment animal models, the VSVΔG-SUDV GP and VSVΔG-BDBV GP systems represent essential tools for accelerating countermeasure development. Future research integrating transcriptomic, proteomic, and immunological analyses in these models will help delineate host–virus interactions specific to non-Zaire ebolaviruses, providing insights into why certain species, such as SUDV, elicit distinct immune and pathological profiles. This platform may facilitate experimental investigation of GP-dependent infection and therapeutic evaluation in a defined surrogate system.

ACKNOWLEDGEMENTS

We thank the Wuhan Center for Experimental Animals and the Institutional Center for Shared Technologies and Facilities for their excellent technical assistance and support in animal experiments and instrumentation.

SUPPLEMENTARY DATA

Supplementary data to this article can be found online.

COMPETING INTERESTS

The authors declare that they have no competing interests.

AUTHORS' CONTRIBUTIONS

S.C. conceived the overall project and provided strategic supervision throughout the study. X.H.Z. and F.H.Y. contributed to experimental design, coordinated project execution, and ensured data integrity. S.C. and X.H.Z. secured funding. B.Y.Z., F.X.L., X.H.Z., J.H.Z., Y.W., W.J.L. and Y.X. performed the experiments and analyzed the data. J.G.Z. generated, optimized, and validated the monoclonal antibody panel used in this study. S.W. rescued and characterized the viruses. B.Y.Z. and X.H.Z. wrote and revised the manuscript. All authors read and approved the final version of the manuscript.

REFERENCES

Bradfute SB, Braun DR, Shamblin JD, et al. 2007. Lymphocyte death in a mouse model of Ebola virus infection. *The Journal of infectious diseases*, **196 S2**: S296–S304.

Bradfute SB, Swanson PE, Smith MA, et al. 2010. Mechanisms and consequences of ebolavirus-induced lymphocyte apoptosis. *The Journal of immunology*, **184**(1): 327–335.

Dong F, Li D, Wen D, et al. 2019. Single dose of a rVSV-based vaccine elicits complete protection against severe fever with thrombocytopenia syndrome virus. *NPJ Vaccines*, **4**(1): 5.

Emanuel J, Callison J, Dowd KA, et al. 2018. A VSV-based Zika virus vaccine protects mice from lethal challenge. *Scientific reports*, **8**(1): 11043.

Fang XK, Zhang SK, Sun XD, et al. 2012. Evaluation of attenuated VSVs with mutated M or/and G proteins as vaccine vectors. *Vaccine*, **30**(7): 1313–1321.

Formenty P, Hatz C, Le Guenno B, et al. 1999. Human infection due to Ebola virus, subtype Côte d'Ivoire: clinical and biologic presentation. *The Journal of infectious diseases*, **179 S1**: S48–S53.

Geisbert TW, Young HA, Jahrling PB, et al. 2003. Pathogenesis of Ebola hemorrhagic fever in primate models: evidence that hemorrhage is not a direct effect of virus-induced cytolysis of endothelial cells. *The American journal of pathology*, **163**(6): 2371–2382.

Gilchuk P, Murin CD, Cross RW, et al. 2021. Pan-ebolavirus protective therapy by two multifunctional human antibodies. *Cell*, **184**(22): 5593–5607.18.

Hicks P, Manzoni TB, Westover JB, et al. 2024. Safety, Immunogenicity, and Efficacy of a Recombinant Vesicular Stomatitis Virus Vectored Vaccine Against Severe Fever with Thrombocytopenia Syndrome Virus and Heartland Bandavirus. *Vaccines*, **12**(12): 1403.

Iluz-Freundlich D, Grubert Van Iderstine M, Uhanova J, et al. 2021. Low serum alkaline phosphatase levels in patients with chronic liver diseases: Possible contributions to disease pathogenesis. *Clinics and research in hepatology and gastroenterology*, **45**(4): 101694.

Jiménez-Cabello L, Utrilla-Trigo S, Benavides-Silván J, et al. 2024. IFNAR(-/-) Mice Constitute a Suitable Animal Model for Epizootic Hemorrhagic Disease Virus Study and Vaccine Evaluation. *International journal of biological sciences*, **20**(8): 3076–3093.

Languon S, Quaye O. 2019. Filovirus Disease Outbreaks: A Chronological Overview. *Virology: Research and Treatment*, **10**: 1178122x19849927.

Lemmens V, Kelchtermans L, Debaveye S, et al. 2023. YF17D-vectored Ebola vaccine candidate protects mice against lethal surrogate Ebola and yellow fever virus challenge. *NPJ Vaccines*, **8**(1): 99.

Lennemann NJ, Herbert AS, Brouillette R, et al. 2017. Vesicular Stomatitis Virus Pseudotyped with Ebola Virus Glycoprotein Serves as a Protective, Noninfectious Vaccine against Ebola Virus Challenge in Mice. *Journal of virology*, **91**(17): e00479–17.

Li WJ, Yang WY, Liu XQ, et al. 2024. Fully human monoclonal antibodies against Ebola virus possess complete protection in a hamster model. *Emerging microbes & infections*, **13**(1): 2392651.

Martines RB, Ng DL, Greer PW, et al. 2015. Tissue and cellular tropism, pathology and pathogenesis of Ebola and Marburg viruses. *The Journal of pathology*, **235**(2): 153–174.

Marzi A, Emanuel J, Callison J, et al. 2018. Lethal Zika Virus Disease Models in Young and Older Interferon α/β Receptor Knock Out Mice. *Frontiers in cellular and infection microbiology*, **8**: 117.

Mcelroy AK, Erickson BR, Flietstra TD, et al. 2014. Ebola hemorrhagic

Fever: novel biomarker correlates of clinical outcome. *The Journal of infectious diseases*, **210**(4): 558–566.

Meyts I, Casanova JL. 2021. Viral infections in humans and mice with genetic deficiencies of the type I IFN response pathway. *European journal of immunology*, **51**(5): 1039–1061.

Mishra AR, Byrareddy SN, Nayak D. 2020. IFN-I Independent Antiviral Immune Response to Vesicular Stomatitis Virus Challenge in Mouse Brain. *Vaccines (Basel)*, **8**(2): 326.

Ramakrishnan MA. 2016. Determination of 50% endpoint titer using a simple formula. *World journal of virology*, **5**(2): 85–86.

Sah R, Hada V, Mohanty A, et al. 2023. Re-emergence of Sudan ebolavirus after a decade: new challenge to Ebola control. *International journal of surgery*, **109**(2): 131–133.

Saito T, Maruyama J, Nagata N, et al. 2020. A Surrogate Animal Model for Screening of Ebola and Marburg Glycoprotein-Targeting Drugs Using Pseudotyped Vesicular Stomatitis Viruses. *Viruses*, **12**(9): 923.

Sanchez A, Lukwiya M, Bausch D, et al. 2004. Analysis of human peripheral blood samples from fatal and nonfatal cases of Ebola (Sudan) hemorrhagic fever: cellular responses, virus load, and nitric oxide levels. *Journal of virology*, **78**(19): 10370–10377.

Siragam V, Wong G, Qiu XG. 2018. Animal models for filovirus infections. *Zoological research*, **39**(1): 15–24.

Sivanandy P, Jun PH, Man LW, et al. 2022. A systematic review of Ebola virus disease outbreaks and an analysis of the efficacy and safety of newer drugs approved for the treatment of Ebola virus disease by the US Food and Drug Administration from 2016 to 2020. *Journal of infection and public health*, **15**(3): 285–292.

Spengler JR, Welch SR, Ritter JM, et al. 2023. Mouse models of Ebola virus tolerance and lethality: characterization of CD-1 mice infected with wild-type, guinea pig-adapted, or mouse-adapted virus. *Antiviral research*, **210**: 105496.

Urbanowicz RA, Mcclure CP, Sakuntabhai A, et al. 2016. Human Adaptation of Ebola Virus during the West African Outbreak. *Cell*, **167**(4): 1079–1087. e5.

Wang S, Li WJ, Wang ZS, et al. 2024. Emerging and reemerging infectious diseases: global trends and new strategies for their prevention and control. *Signal transduction and targeted therapy*, **9**(1): 223.

Wang S, Wang ZS, Wang WQ, et al. 2025. A VSV-based oral rabies vaccine was sentineled by Peyer's patches and induced a timely and durable immune response. *Molecular therapy*, **33**(4): 1701–1719.

Wang S, Zhang C, Liang B, et al. 2022. Characterization of Immune Response Diversity in Rodents Vaccinated with a Vesicular Stomatitis Virus Vectored COVID-19 Vaccine. *Viruses*, **14**(6): 1127.

Wong G, Qiu XG. 2018. Type I interferon receptor knockout mice as models for infection of highly pathogenic viruses with outbreak potential. *Zoological research*, **39**(1): 3–14.

Yang WY, Li WJ, Zhou WJ, et al. 2024. Establishment and application of a surrogate model for human Ebola virus disease in BSL-2 laboratory. *Virologica Sinica*, **39**(3): 434–446.

Zhang HQ, Zhang ZR, Deng CL, et al. 2024. A lethal mice model of recombinant vesicular stomatitis viruses for EBOV-targeting prophylactic vaccines evaluation. *Virologica Sinica*, **39**(3): 516–519.

Zhou JH, Zhang XH, Yao YF, et al. 2025. Recombinant live attenuated measles virus-based vaccines inducing comprehensive protection against Ebola and Marburg viruses. *Molecular therapy*, **33**(11): 5470–5488.